In Situ Observation of Transient Evolution of Inclusions by Ca Treatment in Molten Steel

YEGUANG WANG and CHENGJUN LIU

On the basis of preparing the samples containing various single types of inclusions, the novel experiments using confocal laser scanning microscopy were designed to *in situ* observe the transient evolution of inclusions morphology and size during the modification process from Al_2O_3 and $MgO–Al_2O_3$ to low-melting point $CaO–Al_2O_3–(MgO)$, in which the disaggregation of large-sized Al_2O_3 clusters by Ca treatment was detected for the first time, resulting in the reduce of inclusions size in melts.

https://doi.org/10.1007/s11663-022-02606-2

THE characteristics of nonmetallic inclusions are expected to significantly affect the production process and the product quality of steel. The problem of nozzle clogging, for instance, is caused by the deposition of large-sized inclusions and clusters with high melting point on the inner wall of submerged entry nozzle, which leads to unstable casting and causes crack defects on slab.[1–4]

Aluminum is one of the most popular deoxidizers because of its strong affinity to oxygen, thereby a large number of Al_2O_3 formed in molten steel. Mg was usually introduced to the Al-killed molten steel from refining slag or refractory containing MgO.[5,6] Many studies have proposed that trace amount of Mg was sufficient to modify Al_2O_3 to $MgO–Al_2O_3$ through theoretical calculations and experiments.[7,8] Although inclusions sizes can be reduced by means of this modification, both Al_2O_3 and $MgO–Al_2O_3$ are inclusions with the characteristic of high melting point and high hardness, which caused nozzle clogging problem and product quality defects.[9–11] In order to alleviate the harm of these inclusions, Ca treatment has been widely used to modify them to calcium aluminate in the liquid phase. Many studies were performed to discuss the thermodynamic,[12] kinetics,[13–15] and evolution mechanism[16] for the modification process in Al–Mg–Ca–O deoxidized steel under both laboratory scale experiments and industrial trials. However, these studies mainly investigated the inclusion information through *postmortem* analysis in quenched high-temperature samples.

The technology of confocal laser scanning microscopy (CLSM) originated in the 1980s is capable of observing *in situ* experimental phenomena at high temperature, so as to directly reflect the characteristics of inclusions. The precipitation behavior of inclusions during steel solidification[17] and agglomeration behavior of various inclusions caused by capillary interaction[18–21] were investigated by using CLSM. However, due to the lack of inclusions control during observation and the limitations of CLSM experimental methods, the transient evolution of inclusions characteristics during its modification, especially the transition from solid inclusions to liquid ones, has not been investigated by *in situ* observation yet.

In the present work, the alloy chosen is Fe–21Cr–11Ni stainless steel, in which Al_2O_3 and $MgO–Al_2O_3$ inclusions were expected to be modified to the liquid phase because of their harm to casting process and products quality. To avoid the interference between different kinds of inclusions in the *in situ* observation, the samples containing a single type of inclusions (Al_2O_3 or $MgO–Al_2O_3$) and the sample with Ca treatment were prepared according to thermodynamic calculation. Then, the novel CLSM experiments were carried out to document and quantify the evolution of inclusions from solid phase to liquid ones, with an emphasis on their sizes change.

Thermodynamic calculation was performed by FactSage 8.1 software and thereby the stability phase diagram of inclusions was evaluated in Fe–21Cr–11Ni–Al–Ca–(0.0008 Mg)–O melts at 1873 K (1600 °C). Figure 1(a) shows that Al_2O_3, CaO, $CaO–Al_2O_3$ solid and liquid oxides are in equilibrium with molten steel in the Ca and Al contents ranging from 5×10^{-6} to 0.005

YEGUANG WANG and CHENGJUN LIU are with the Key Laboratory for Ecological Metallurgy of Multimetallic Ores, Ministry of Education, Shenyang 110819, Liaoning, P.R. China and also with the School of Metallurgy, Northeastern University, Mailbox 288#, No. 11, Alley 3, Wenhua Road, Heping District, Shenyang 110819, Liaoning, P.R. China. Contact e-mail: liucj@smm.neu.edu.cn

Manuscript submitted February 8, 2022; accepted July 13, 2022.
Article published online August 10, 2022.

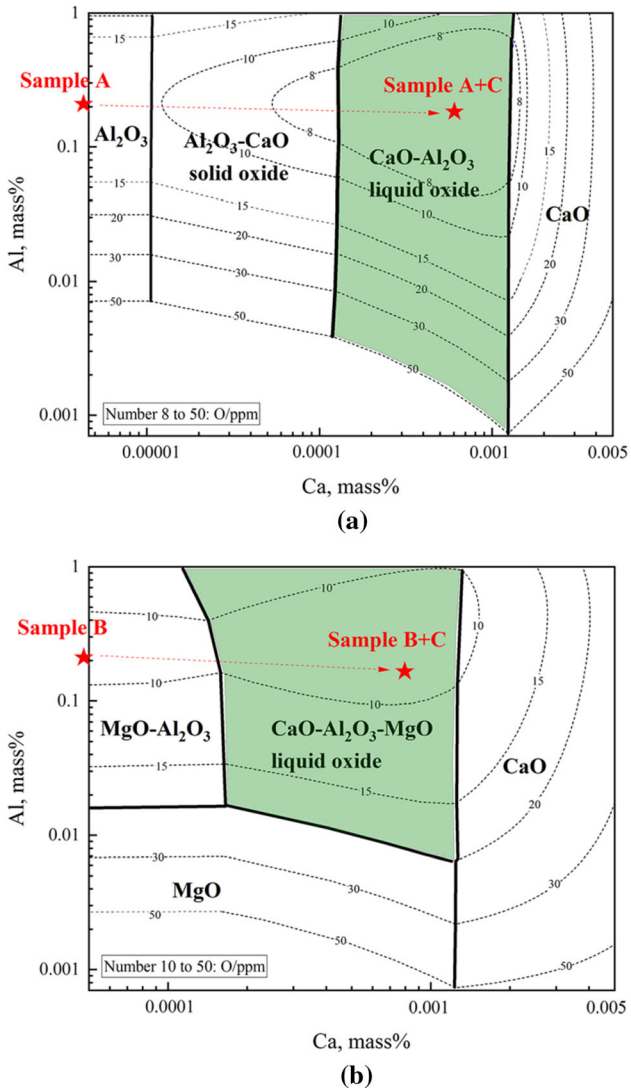

Fig. 1—Calculated inclusion stability diagram of the Fe–21Cr–11Ni–Al–Ca–Mg–O melts at 1873 K: (*a*) without Mg; (*b*) with 0.0008 pct Mg.

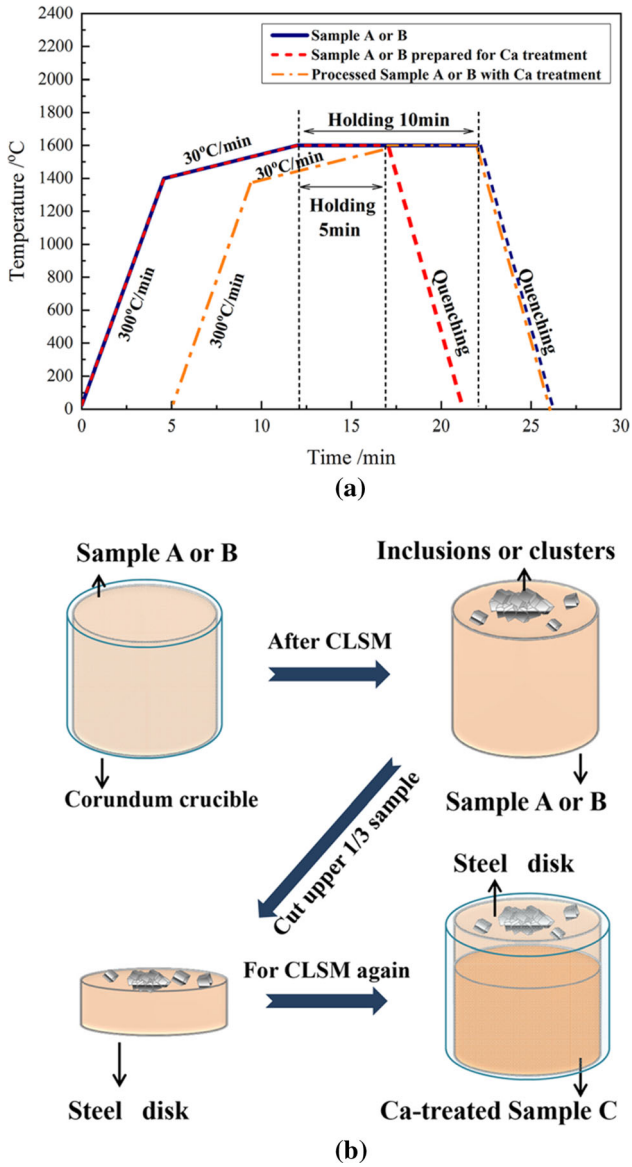

Fig. 2—Schematic of CLSM experiments: (*a*) temperature profile; (*b*) method of samples processing.

pct, and 0.001 to 1 pct. When the melt contains 0.001 pct of Mg, Al_2O_3 and Al_2O_3–CaO solid oxide are replaced by MgO–Al_2O_3 and MgO, as shown in Figure 1(b). Approximately 0.0002 to 0.001 pct of Ca is sufficient to modify the inclusions to CaO–Al_2O_3 liquid oxide in both two melts.

On the basis of thermodynamic calculation, the steel samples containing Al_2O_3 or MgO–Al_2O_3 inclusions were prepared at 1873 K (1600 °C) in a $MoSi_2$ furnace under argon atmosphere. Different amounts of Al, Mg, and Ca were added into the melts containing a certain amount of electrolytic iron, chromium metal, and electrolytic nickel, and then sampled after 30 min to achieve sufficient homogenization of the melts. The details of the experimental operation were described in detail in other literature.[22] In the current work, sample A was deoxidized by Al, Mg treatment after Al deoxidation was used in sample B. Sample C was only treated with Ca and without Al and Mg addition.

The *in situ* observation of inclusions in the above samples was carried out in CLSM (Lasertec VL2000DX), which is equipped with a He–Ne laser and an infrared image furnace. Prior to heating, the chamber was filled with high-purity Ar gas (purity > 99.999 pct) at a constant flow of 50 to 60 mL/min to evacuate the air. The cycle of vacuum and purging with Ar was performed three times to clean the chamber thoroughly. The temperature profile of experiments is shown in Figure 2(a). First, samples A and B were heated to 1873 K (1600 °C) with a heating rate of 300 °C/min. During the 10 min holding time, the inclusions behavior in molten steel was recorded by the CRT monitor at a rate of 30 frames per second. After observation, the heating power was directly turned off so as to quench the samples immediately and retain the characteristics of inclusions at high temperature. Subsequently, another sample A or B was heated in the

Table I. Chemical Analyses of Experimental Samples (Mass Percent, Pct)

Samples	Cr	Ni	Al	Mg	Ca	T.O
A (Al Deoxidation Only)	21.20	11.20	0.22	—	—	0.0029
B (Al/Mg Deoxidation)	21.30	10.90	0.19	0.0011	—	0.0032
C (Ca Treatment Only)	20.90	11.10	0.001	—	0.0007	0.0021
A + C (After Observation)	20.90	11.10	0.19	—	0.0006	0.0034
B + C (After Observation)	21.00	10.90	0.17	0.0008	0.0007	0.0036

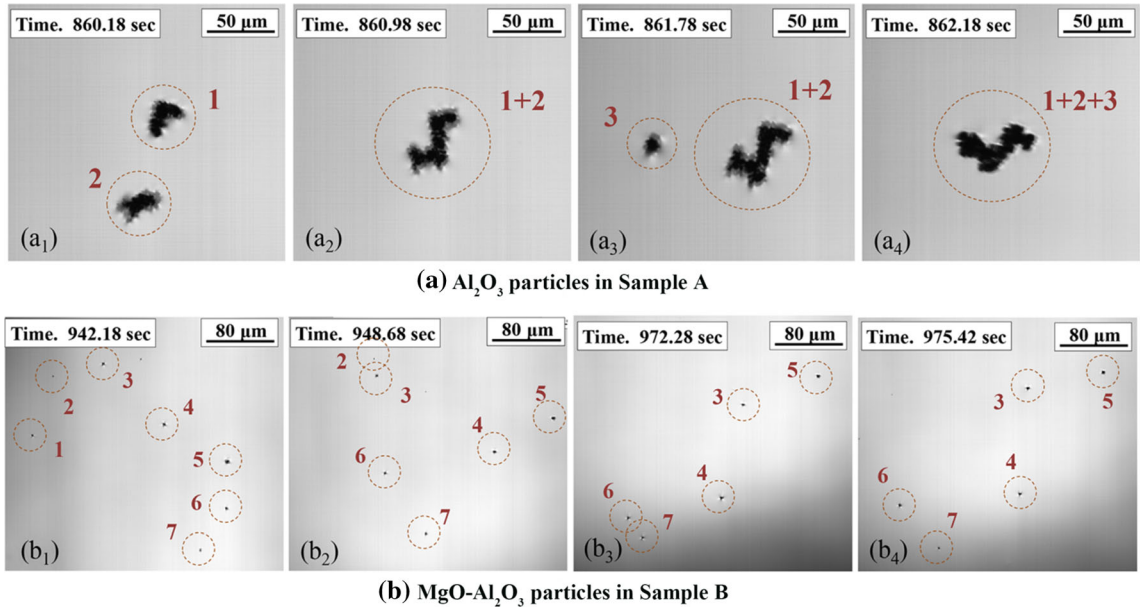

Fig. 3—Images from the *in situ* observation of pure inclusions (*a*) Al_2O_3 particles in Sample A at 860.18 s (a_1), at 860.98 s (a_2) at 861.78 s (a_3), at 862.18 s (a_4); (*b*) MgO-Al_2O_3 particles in Sample B at 942.18 s (b_1), at 948.68 s (b_2), at 972.28 s (b_3), and at 975.42 s (b_4).

same way and quenched immediately after observing for 5 min (corresponding to the red-dotted line in Figure 2(a)), which was then processed to prepare for the following CLSM experiment of Ca treatment, and the processing method is shown in detail in Figure 2(b). A large number of inclusions and agglomerated clusters were floated up to the sample surface during observation. Thus the steel disks containing inclusions and clusters can be obtained by cutting the upper third of the quenched samples. Then the steel disks containing the inclusions or clusters from sample A and B were placed on the surface of Ca-treated sample C to form sample A + C and B + C, respectively, and the inclusion behavior was observed *in situ* in the next 5 min (corresponding to the green-dotted line in Figure 2(a)). After observation, the quenched samples were cross sectioned and polished, for analyzing the morphology and chemical composition of the inclusions by SEM–EDS. The compositions of samples before and after *in situ* observation were determined by ICP-OES with an accuracy of ± 0.5 ppm, as shown in Table I, which are marked as red star in Figure 1, indicating that the experimental results were in accord with the theoretical design, that is, the main inclusions in samples A and B should be Al_2O_3 and MgO–Al_2O_3, respectively, and the compositions of inclusions after Ca treatment were entered into the region of liquid oxide.

The behaviors of various inclusions in molten steel were observed *in situ*. Figure 3(a) shows the agglomeration process of Al_2O_3 inclusions in sample A. Two solid particles with cluster shapes attracted each other to form clusters 1 + 2, then particle 3 moved rapidly towards clusters 1 + 2, and a larger cluster of inclusions consisting of 1 + 2 + 3 was formed in 0.4 s. MgO–Al_2O_3 inclusions in sample B were very small and tended to be dispersed, and non-agglomeration behavior among them within 34 s is exampled in Figure 3(b). Seven inclusions are randomly distributed in molten steel over time. Even though the distance between inclusions 6 and 7 was shortened to less than 20 μm shown in Figure 3(b_3), they did not further agglomerate, but moved away from each other to a distance of about 60 μm shown in Figure 3(b_4).

In Ca-treated sample A, two typical variations of inclusion characteristics were captured, which were determined by the reaction between Al_2O_3 inclusions and Ca shortly after the sample melting. It is obvious from Figures 4(a_1) to (a_4) that a solid inclusion with irregular shape gradually transformed into typical spherical liquid inclusions in about 10 s. In addition,

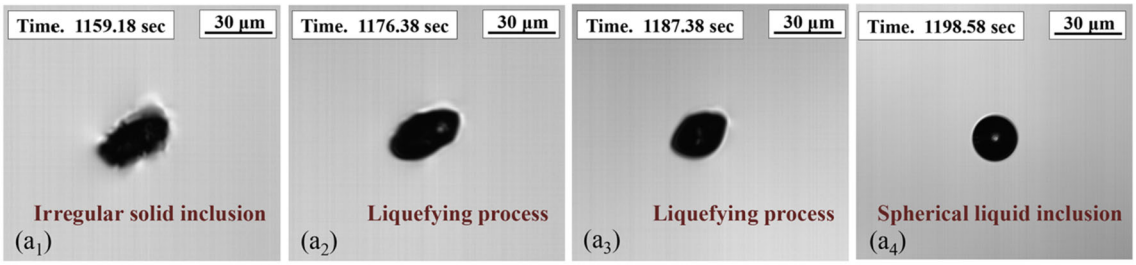

(a) Liquefying process of Al_2O_3 in Sample A+C

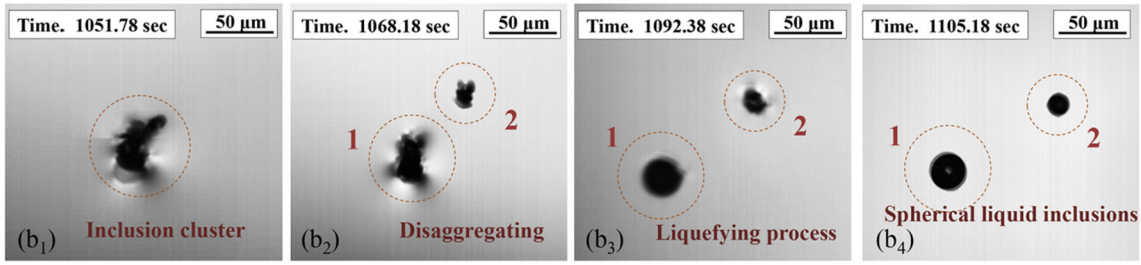

(b) Disaggregation and liquefying process of Al_2O_3 in Sample A+C

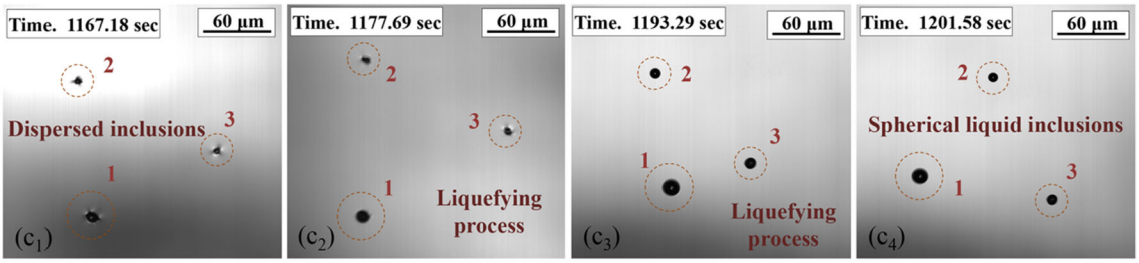

(c) Liquefying process of MgO-Al_2O_3 in Sample B+C

Fig. 4—Images from the *in situ* observation of inclusions modification after Ca treatment (*a*) liquefying process of Al_2O_3 inclusions in Sample A + C at 1159.18 s (a_1), at 1176.38 s (a_2), at 1187.38 s (a_3), at 1198.58 s (a_4); (*b*) disaggregating and liquefying process of inclusions in Sample A + C at 1051.78 s (b_1), at 1068.18 s (b_2), at 1092.38 s (b_3), at 1105.18 s (b_4); (*c*) liquefying process of MgO-Al_2O_3 inclusions in Sample B + C at 1167.18 s (c_1), at 1177.69 s (c_2), at 1193.29 s (c_3), at 1201.58 s (c_4).

some of the large-sized clusters first disaggregated into smaller size inclusions and then gradually transformed to spherical ones, as shown in Figures 4(b_1) to (b_4). The agglomeration force derived from cavity bridge force is known to the main mechanism of inclusions agglomeration, which is significantly affected by the wettability between inclusions and molten steel.[23,24] The disaggregation phenomena of inclusions may be mainly due to the wettability increasing of inclusions during their transformation caused by Ca treatment. The evolution behavior of inclusions in Ca-treated sample B is represented by Figures 4(c_1) to (c_4), in which three irregularly shaped MgO–Al_2O_3 inclusions with smaller size were successively liquefied into spherical inclusions within 30 s. It is worth mentioning that the spherical liquid inclusions formed after Ca treatment in both sample A and B did not agglomerate over time.

The morphology and composition of the inclusions in quenched samples after observation were analyzed by SEM–EDS. As shown in Figure 5(a), the large-sized cluster of Al_2O_3 in sample A was composed of numerous small-sized ones. The small-sized MgO–Al_2O_3 inclusions shown in Figure 5(b) were distributed in sample B, indicating that even though the distance between them is < 4 μm, the two clusters still did not agglomerate further. After Ca treatment, the complex inclusion with MgO–Al_2O_3 core wrapped by CaO–Al_2O_3 shell was detected in sample B + C as shown in Figure 5(c). Yang *et al.*[25] proposed that due to the limitation of kinetic conditions, MgO–Al_2O_3 with large size was difficult to be completely modified to liquid CaO–Al_2O_3 inclusions, instead of forming the complex inclusions similar to those in this work. In addition, Figure 5(d) shows the typical characteristic of liquid CaO–Al_2O_3–(MgO) inclusions dispersed in both samples A + C and B + C, these inclusions were modified from Al_2O_3 and MgO–Al_2O_3.

Figure 6 presents the variation of average size (calculated by the equivalent diameter) of inclusion particles with respect to time. The average size of Al_2O_3 inclusion increased gradually with the increase of time, and its maximum value was 26.57 μm, which agglomerate to form large-sized clusters due to the strong attractive force caused by capillary interaction between them presented in the previous study.[20,21,26] On the contrary, the attractive force between the dispersed MgO–Al_2O_3

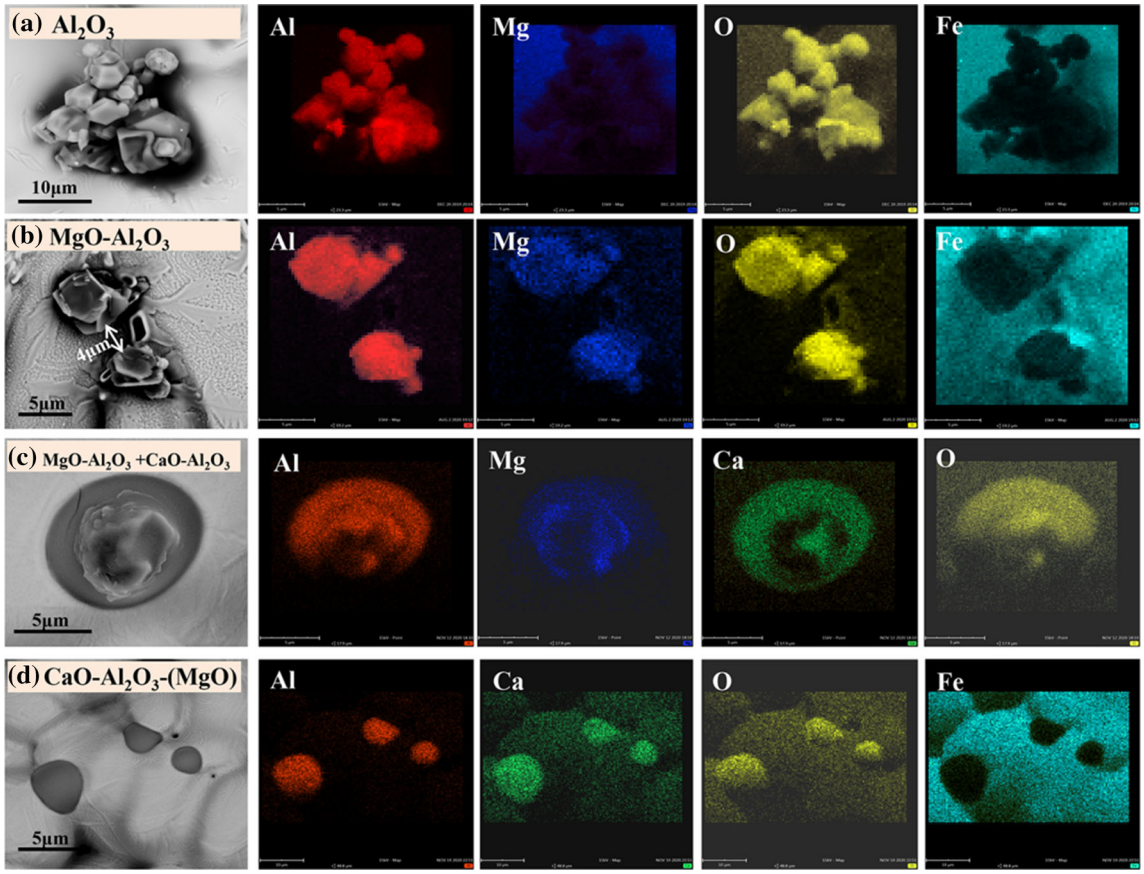

Fig. 5—The composition and morphology of typical inclusions after *in situ* observation: (*a*) pure Al_2O_3 cluster in sample A; (*b*) pure MgO-Al_2O_3 in sample B; (*c*) complex inclusions with MgO-Al_2O_3 core wrapped by CaO-Al_2O_3 shell in sample B + C; (*d*) liquid CaO-Al_2O_3-(MgO) in samples A + C and B + C.

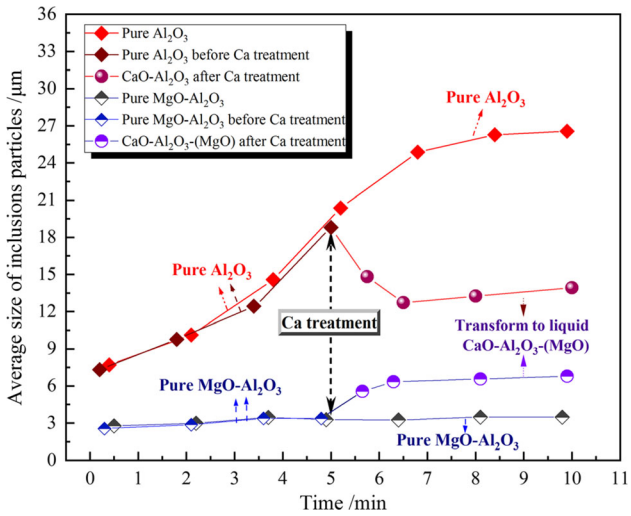

Fig. 6—The variation of inclusion average size with respect to time.

inclusions was weak,[26] which leads to no significant increase of their size in this study. After Ca treatment, the size of inclusions particles decreased significantly from 18.79 to 12.71 μm caused by the modification from Al_2O_3 to CaO–Al_2O_3 liquid inclusions. Ferreira *et al.*[27] and Verma *et al.*[28] proposed that the size of Al_2O_3 clusters can be reduced after Ca treatment, and two possible explanations for which were that new inclusions with smaller size precipitated, or new calcium aluminates formed from the disaggregation of the original clusters. The phenomenon of *in situ* observation shown in Figure 4(a) combined with statistics of inclusions size changes here conformed to the latter explanation. The transformation from MgO–Al_2O_3 to CaO–Al_2O_3–(MgO) liquid inclusions led to size increase, which probably due to the formation of the complex inclusions shown in Figure 5(c), and whose size was still smaller than that from modification of Al_2O_3. Moreover, the size of liquid inclusions was slightly increased because of the weak attractive force among them that was reported in other literatures.[29]

To sum up, the various inclusions (Al_2O_3 and MgO–Al_2O_3) were controlled and obtained in samples by thermodynamic calculation, and the sample containing less than 0.001 pct of Ca that was capable of modifying these inclusions to CaO–Al_2O_3–MgO liquid inclusions. On this basis, a novel CLSM experiment was designed to simulate the modification process from high-melting point inclusions to liquid ones by Ca treatment, in which the transient evolution of the inclusions especially their sizes change, can be observed in situ in molten steel. The pure Al_2O_3 inclusions particles agglomerated rapidly to form large-sized

clusters. On the contrary, the $MgO–Al_2O_3$ inclusions were easy to be dispersed in molten steel. After Ca treatment, the irregularly shaped Al_2O_3 were transformed to spherical liquid $CaO–Al_2O_3$, and the average size of them decreased from 18.79 to 12.71 μm owing to the disaggregation of the former Al_2O_3 clusters. For some of $MgO–Al_2O_3$ inclusions with large size, Ca treatment was unable to completely modify them, resulting in the formation of the complex inclusions with $MgO–Al_2O_3$ core wrapped by $CaO–Al_2O_3$ shell. The inclusions size after modification of $MgO–Al_2O_3$ was much smaller than that of modifying Al_2O_3. Once the liquid inclusions were formed, their size no longer increased significantly due to non-agglomeration among them. The CLSM experimental method proposed in this study is expected to be performed to investigate the transient evolution of other inclusions in the future.

This work was supported by the National Key R&D Program of China [No. 2017YFC0805100], NSFC-Liaoning Joint Fund [U1908224], National Natural Science Foundation of China [NSFC, No. 51874082].

On behalf of all authors, the corresponding author states that there is no conflict of interest.

REFERENCES

1. L.A. Frank: *Ironmak. Steelmak.*, 1999, vol. 26, pp. 33–39.
2. R.B. Tuttle, J.D. Smith, and K.D. Peaslee: *Metall. Mater. Trans. B*, 2005, vol. 36B, pp. 885–92.
3. P. Kaushik, J. Lehmann, and M. Nadif: *Metall. Mater. Trans. B*, 2012, vol. 43B, pp. 710–25.
4. B.A. Webler and P.C. Pistorius: *Mater. Trans. B*, 2020, vol. 51B, pp. 2437–52.
5. C. Liu, M. Yagi, X. Gao, S.J. Kim, F. Huang, S. Ueda, and S. Kitamura: *Metall. Mater. Trans. B*, 2018, vol. 49B, pp. 113–22.
6. H.J. Wang, G. Björn, and D. Sichen: *Metall. Mater. Trans. B*, 2015, vol. 46B, pp. 749–57.
7. K. Fujii, T. Nagasaka, and M. Hino: *ISIJ Int.*, 2000, vol. 40, pp. 1059–1066.
8. J.H. Park: *Metall. Trans. B*, 2007, vol. 38B, pp. 657–63.
9. J.H. Park and H. Todoroki: *ISIJ Int.*, 2010, vol. 50, pp. 1333–46.
10. L. Zhang and B.G. Thomas: *ISIJ Int.*, 2003, vol. 43, pp. 271–91.
11. H. Todoroki and S. Inada: *Bull. ISIJ*, 2003, vol. 8, p. 575.
12. G. Yang, X. Wang, F. Huang, P. Wei, and X. Hao: *Metall. Mater. Trans. B*, 2015, vol. 46B, pp. 145–54.
13. W. Yang, L. Zhang, X. Wang, Y. Ren, X. Liu, and Q. Shan: *ISIJ Int.*, 2013, vol. 53, pp. 1401–10.
14. J.H. Park and L. Zhang: *Metall. Trans. B*, 2020, vol. 51B, pp. 2453–82.
15. Y. Tabatabaei, K.S. Coley, G.A. Irons, and S. Sun: *Metall. Mater. Trans. B*, 2018, vol. 49B, pp. 2744–56.
16. M. Lind and L. Holappa: *Metall. Mater. Trans. B*, 2010, vol. 41B, pp. 359–66.
17. S. Kimura, K. Nakajima, S. Mizoguchi, and H. Hasegawa: *Metall. Mater. Trans. A*, 2002, vol. 33A, pp. 427–36.
18. W. Mu, N. Dogan, and K.S. Coley: *Metall. Mater. Trans. B*, 2017, vol. 48B, pp. 2379–88.
19. W. Mu, N. Dogan, and K.S. Coley: *Metall. Mater. Trans. B*, 2017, vol. 48B, pp. 2092–103.
20. W. Mu and C. Xuan: *Metall. Mater. Trans. B*, 2019, vol. 50B, pp. 2694–705.
21. W. Mu, N. Dogan, and K.S. Coley: *JOM*, 2018, vol. 70, pp. 1199–209.
22. Y. Wang and C. Liu: *ISIJ Int.*, 2020, vol. 51, pp. 1–1.
23. K. Sasai: *ISIJ Int.*, 2014, vol. 54, pp. 2780–789.
24. K. Sasai: *ISIJ Int.*, 2016, vol. 56, pp. 1013–1022.
25. S. Yang, Q. Wang, L. Zhang, J. Li, and K. Peaslee: *Metall. Mater. Trans. B*, 2012, vol. 43B, pp. 731–50.
26. S. Kimura, K. Nakajima, and S. Mizoguchi: *Metall. Mater. Trans. B*, 2001, vol. 32B, pp. 79–85.
27. Ferreira Do Nas M E. Inclusions Size Distributions After Calcium Treatment in Low Carbon Aluminum Killed Steels[D]. Carnegie Mellon University, 2018.
28. N. Verma, P.C. Pistorius, R.J. Fruehan, M.S. Potter, H.G. Oltmann, and E.B. Pretorius: *Metall. Mater. Trans. B*, 2012, vol. 43B, pp. 830–40.
29. Y. Kang, B. Sahebkar, P.R. Scheller, K. Morita, and D. Sichen: *Metall. Mater. Trans. B*, 2011, vol. 42B, pp. 522–34.